The Astrophysical Journal, 578:648–656, 2002 October 10

EMISSION LINES OF Fe VII–Fe X IN THE EXTREME ULTRAVIOLET REGION, 60–140 Å

J. K. Lepson
Space Sciences Laboratory, University of California at Berkeley, Grizzly Peak at Centennial Drive, Berkeley, CA 94720; lepson@ssl.berkeley.edu

P. Beiersdorfer, G. V. Brown,[1] D. A. Liedahl, and S. B. Utter
High Temperature Physics Division, Lawrence Livermore National Laboratory, University of California, 7000 East Avenue, Livermore, CA 94550; beiersdorfer@llnl.gov, gvb@milkyway.gsfc.nasa.gov, liedahl1@llnl.gov, e910526@popgun.llnl.gov

N. S. Brickhouse and A. K. Dupree
Smithsonian Astrophysical Observatory, 60 Garden Street, Cambridge, MA 02138; bhouse@head-cfa.harvard.edu, dupree@cfa.harvard.edu

J. S. Kaastra and R. Mewe
Space Research Organization Netherlands, Sorbonnelaan 2, 3584 CA Utrecht, The Netherlands; J.S.Kaastra@sron.nl, R.Mewe@sron.nl

and

S. M. Kahn
Department of Physics, Columbia University, Pupin Hall, 538 West 120th Street, New York, NY 10027; skahn@astro.columbia.edu
Received 2002 May 7; accepted 2002 June 12

ABSTRACT

We report on emission spectra of iron in the extreme ultraviolet recorded at an electron density of $\sim 5 \times 10^{11}$ cm^{-3} at the Lawrence Livermore electron beam ion trap EBIT-II. We present a summary of observed emission lines, including wavelengths and emission intensities. We also illustrate our technique for isolating pure charge states of the desired ion and present spectra of pure Fe VII–Fe X. Our measurements add a large number of newly identified lines to existing line lists in the extreme-ultraviolet region, 60–140 Å. While many of these lines are quite weak, they add up to a significant flux that can seriously affect interpretations of global fitting models, especially when applied to stars with material at the appropriate temperatures, such as Procyon, α Cen, and the Sun.

Subject headings: line: identification — methods: analytical — methods: laboratory — stars: coronae — ultraviolet: stars

1. INTRODUCTION

Accurate and complete spectral models are essential for analyses of spectroscopic data returned by new-generation extreme-ultraviolet and X-ray satellites, such as the *Extreme Ultraviolet Explorer* (*EUVE*), the low energy transmission grating spectrometer (LETGS) on the *Chandra X-Ray Observatory*, and the impending *Cosmic Hot Interstellar Plasma Spectrometer* (*CHIPS*). Deficiencies in currently available data sets in some cases hamper analyses and may result in incorrect interpretations of spectroscopic observations. For example, global fits of the short-wavelength band spectra (80–140 Å) taken with *EUVE*, in which a synthetic spectrum is fitted globally to the observed spectrum, have produced controversial results. In order to fit the apparently high continuum, a strong bremsstrahlung emission component with an unsatisfyingly high temperature on the order of 3×10^7 K had to be invoked (Mewe et al. 1995b). Subsequent laboratory measurements confirmed suggestions by Jordan (1968, 1996), Schmitt, Drake, & Stern (1996), and Drake, Laming, & Widing (1997) that the line lists used in the global fitting models were seriously inadequate. For example, a measurement of Fe IX and Fe X transitions at the Lawrence Livermore National Laboratory's electron beam ion trap EBIT-II showed that roughly 70% of the observed emission between 80 and 140 Å was not accounted for in global fitting models (Beiersdorfer et al. 1999b). To a somewhat lesser extent, this was also true for Fe VII and Fe VIII. It was found that a high density of weak lines in the spectral range from these charge states form a quasi continuum that mimicked the high-temperature bremsstrahlung continuum. However, no line list was given.

In the following we present a detailed line list of Fe VII–Fe X spectra obtained at the Livermore EBIT-II facility. We present wavelengths and relative intensities of individual features observed in the spectra with an accuracy of 0.02 Å. We compare our results with predictions from published line lists and also present new calculations to complement our measurements. The result is a listing of emission lines from Fe VII to Fe X over the 60–140 Å range, including wavelengths, relative intensities, and identifications, which significantly augments the currently existing atomic database for these ions.

With this database we hope to provide the spectroscopic information necessary to produce overall synthetic spectra that can be used in global fitting. This database should also provide for spectral fits and line identifications with higher reliability, particularly for late-type stars with relatively cool coronae, such as the Sun, α Cen, and Procyon.

2. SPECTROSCOPIC MEASUREMENTS

Measurements were taken on the Lawrence Livermore electron beam ion trap EBIT-II (Beiersdorfer et al. 2000). EBIT-II is uniquely suited for such investigations because it can be operated at the very low voltages (100–300 eV) necessary to produce the low charge states we investigated. Moreover, different charge states are produced simply by changing the voltage of the electron beam. As the voltage

[1] Current address: Goddard Space Flight Center, Greenbelt, MD 21201.

increases, a higher charge state appears when the ionization potential is exceeded, and lower charge states decline and disappear as they become ionized. Ideally, charge states appear one by one as the voltage increases. In practice, there is some mixing because of recombination. In addition, the next higher state is sometimes present because of a 30 eV spread in the beam energy, which is comparable to the separation in ionization potentials in the region of interest. The observed balance also somewhat lags the balance that would be expected from a monoenergetic electron beam because neutral iron is continuously injected, the trap is periodically emptied and filled (on the order of 1–3 s), and the measurements are time-integrated over the ionization phase. The typical spectrum thus contains one to three charge states in addition to the dominant one. By systematically recording spectra at different energies and observing the appearance and disappearance of different charge states, however, it is possible to isolate the emission of a single charge state, as we illustrate below.

Spectra were measured with a grazing-incidence spectrometer (Beiersdorfer et al. 1999a) employing an average 1200 line mm^{-1} flat-field grating developed by Harada & Kita (1980; Nakano et al. 1984) with a 3° angle of incidence. Readouts were taken with a back-illuminated, liquid nitrogen–cooled CCD camera with a 1 inch square array of 1024×1024 pixels. The instrumental resolution is ~300 at 100 Å.

Wavelength calibrations were performed using the well-known K-shell emission lines of nitrogen, in particular the N VII Lyα line and the N VI resonance line commonly referred to as *w*, as described by Beiersdorfer et al. (1999a). These lines were observed in the first through seventh orders to calibrate our iron spectra. Calibration spectra were taken periodically throughout the experimental run.

Spectra were also taken without an active trap, i.e., without a potential applied to the trap electrodes. These spectra enabled us to determine the level of background emission (including visible light from the electron-gun filament, to which the CCD camera is sensitive), which was then subtracted from the iron to yield background-corrected spectra. Background measurements were typically taken after every few iron spectra to ensure maximum accuracy in assessing the true iron emission levels.

Figure 1 shows EBIT-II spectra (background subtracted) obtained at beam energies of 145, 200, and 250 eV. The dominant charge states are Fe VIII, Fe IX, and Fe X, respectively, in accordance with the ionization potentials for Fe VII–Fe X of 125, 151, 234, and 262 eV, respectively (Kelly 1987). Note that Fe VII is also present in the Fe VIII spectrum, Fe VII and Fe VIII are present in the Fe IX spectrum, and Fe VII, Fe VIII, and Fe IX are present in the Fe X spectrum.

3. CONSTRUCTION OF SINGLE-ION SPECTRA

Given the large number of lines, attribution of a given feature to the emitting ion can be difficult in spectra that contain more than one charge state. Ideally, we would like to record only spectra from a single charge state to make attribution straightforward. Because we have recorded spectra at different energies with different dominant charge states, we are able to isolate the emission from a single charge state by proper subtraction of neighboring ones, following the procedure described by Lepson et al. (2000).

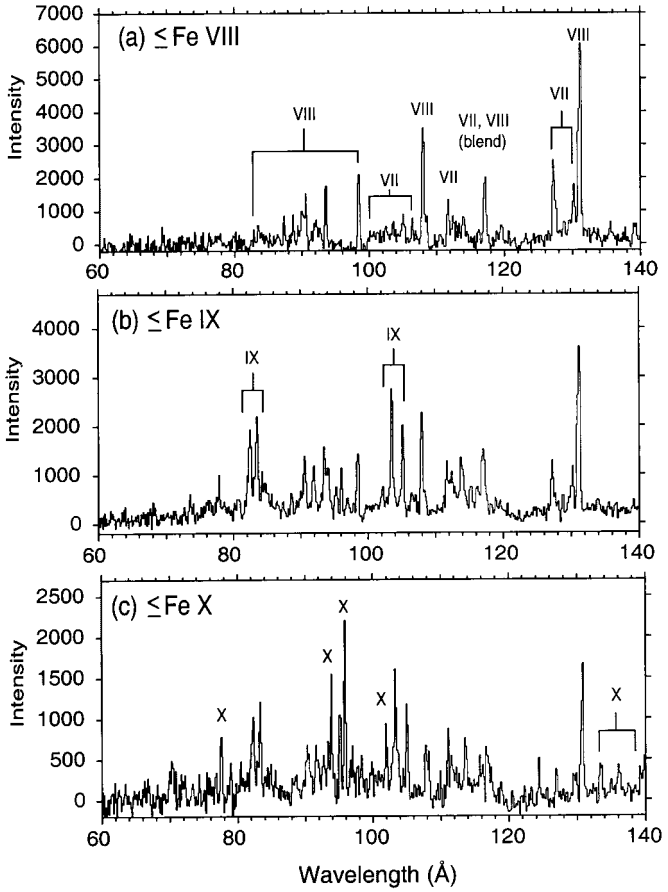

FIG. 1.—Spectra obtained with EBIT-II after subtraction of a constant stray light background. Note that each spectrum includes lines from several charge states. (*a*) Fe VII and Fe VIII (dominant), beam energy 145 eV. (*b*) Fe VII, Fe VIII, and Fe IX (dominant), beam energy 200 eV. (*c*) Fe VII, Fe VIII, Fe IX, and Fe X (dominant), beam energy 200 eV.

The lowest energy spectrum contains both Fe VII and Fe VIII, which can be readily separated by inspection, using published line identifications (Kaastra & Mewe 1993; Kelly 1987) for Fe VIII and the visually apparent Rydberg series for both. The spectra of pure Fe VII and Fe VIII emission are shown in Figures 2 and 3, respectively.

Pure spectra of Fe IX and Fe X were produced by subtracting spectra of the lower charge states from the original mixed spectra. Comparisons of spectra taken at lower and higher energies (Fig. 4) provide a simple visual comparison to help show which peaks belong to the charge state one is attempting to isolate. Because different charge states dominate at different energies, relative peak values differ.

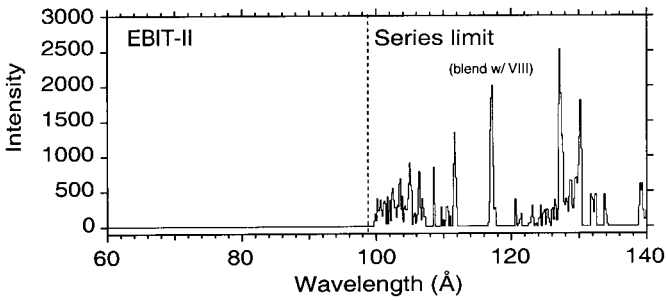

FIG. 2.—Pure Fe VII emission from EBIT-II

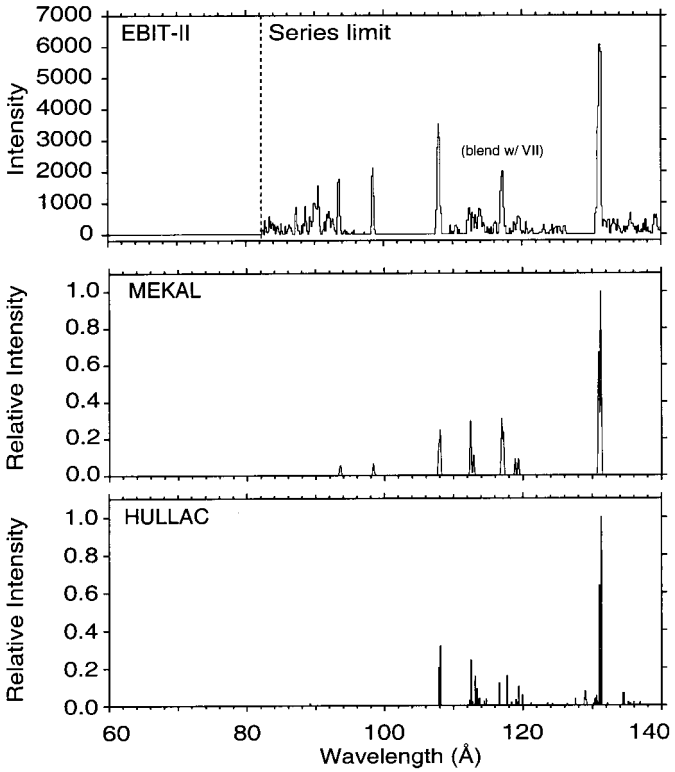

FIG. 3.—Pure Fe VIII emission from EBIT-II compared with synthetic spectra derived from the MEKAL database and HULLAC calculations.

Comparisons with spectra of lower energy show which peaks belong to lower charge states (Fig. 4, *top*), whereas comparisons with spectra of higher energy show which peaks belong to higher charge states (Fig. 4, *bottom*).

Figure 5 illustrates the spectra obtained after subtracting contributions from charge states lower or higher than the one of interest. We first normalize both the pure Fe VII and the mixed Fe IX to the dominant Fe VII peak at 127.3 Å. The Fe VII spectrum is then subtracted from the mixed Fe IX spectrum to result in a mix of Fe VIII, Fe IX, and Fe X (Fig. 5*a*). Similarly, after normalizing to its dominant peak at 131.3 Å, Fe VIII is subtracted to result in a mix of Fe IX and Fe X (Fig. 5*b*). Finally, after normalizing to its dominant peak at 96 Å, Fe X is subtracted to leave pure Fe IX (Fig. 5*c*). The same technique is used to produce pure Fe X.

We note that the subtraction procedure introduces a certain amount of statistical noise into the resulting spectrum. While the increased noise level is clearly undesirable, the advantage of the subtraction procedure is that a reasonably pure spectrum from a single charge state is produced for comparison with calculations and for more apparent line identification. Figures 6 and 7 show the resulting pure spectra of Fe IX and Fe X, respectively.

4. EXTRACTION OF ATOMIC DATA

Peaks from the original spectra, such as those shown in Figure 1, were fitted with Gaussian trial functions to determine line positions and relative intensities. We used the original spectra for fitting purposes in order to avoid any

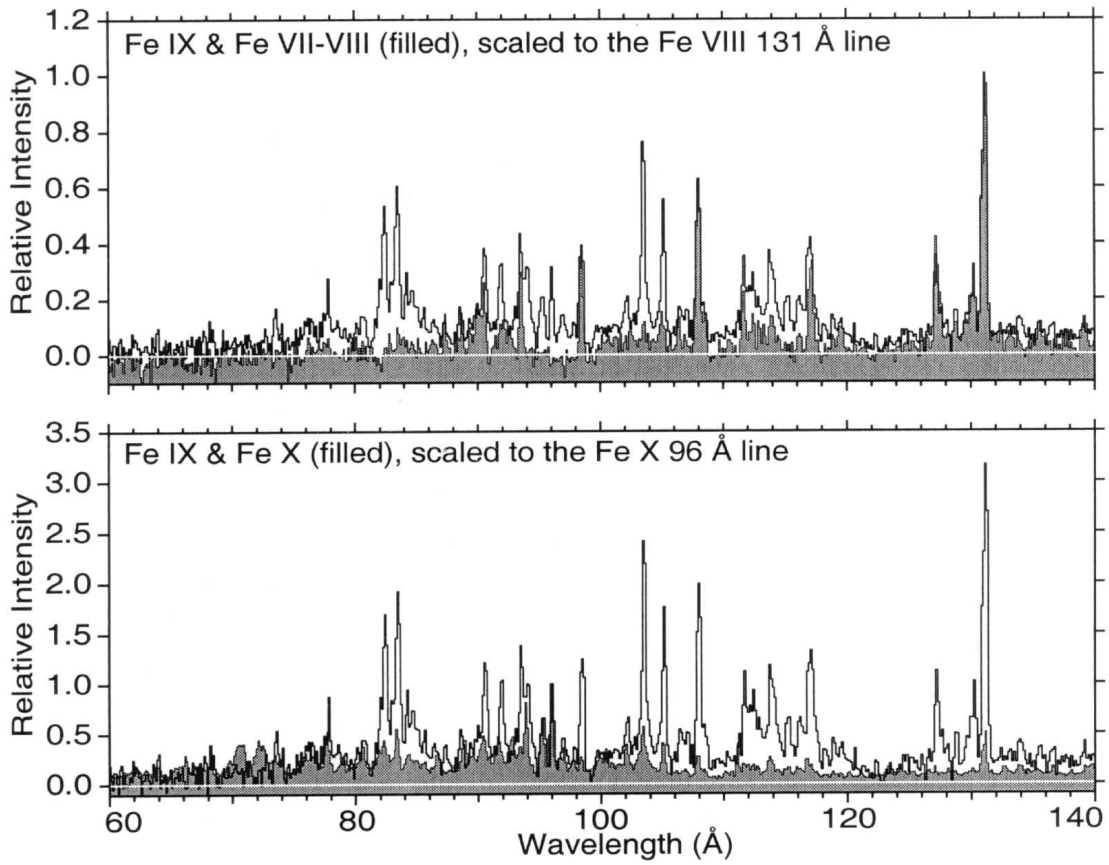

FIG. 4.—Comparison of Fe IX with lower and higher charge states. *Top*: Spectrum dominated by Fe IX (*open curve*) is overlaid with a spectrum recorded at lower energy (*filled curve*), dominated by Fe VII and Fe VIII. *Bottom*: Spectrum dominated by Fe IX (*open curve*) is overlaid with a spectrum recorded at higher energy (*filled curve*), dominated by Fe X.

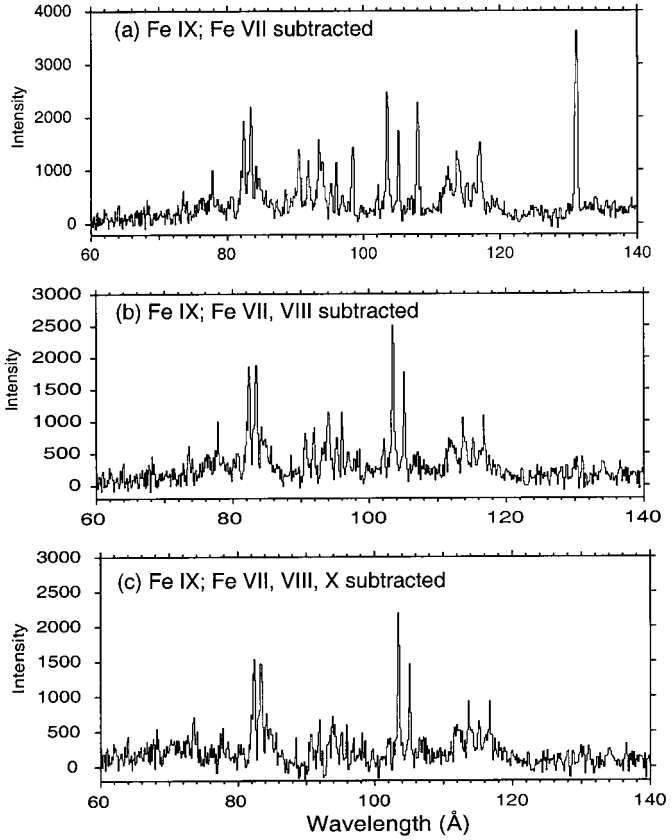

FIG. 5.—Isolation of pure Fe IX emission. (*a*) Subtraction of Fe VII leaves a spectrum composed of Fe VIII, Fe IX, and Fe X. (*b*) Subtraction of Fe VIII leaves a spectrum composed of Fe IX and Fe X. (*c*) Subtraction of Fe X leaves a spectrum composed solely of Fe IX.

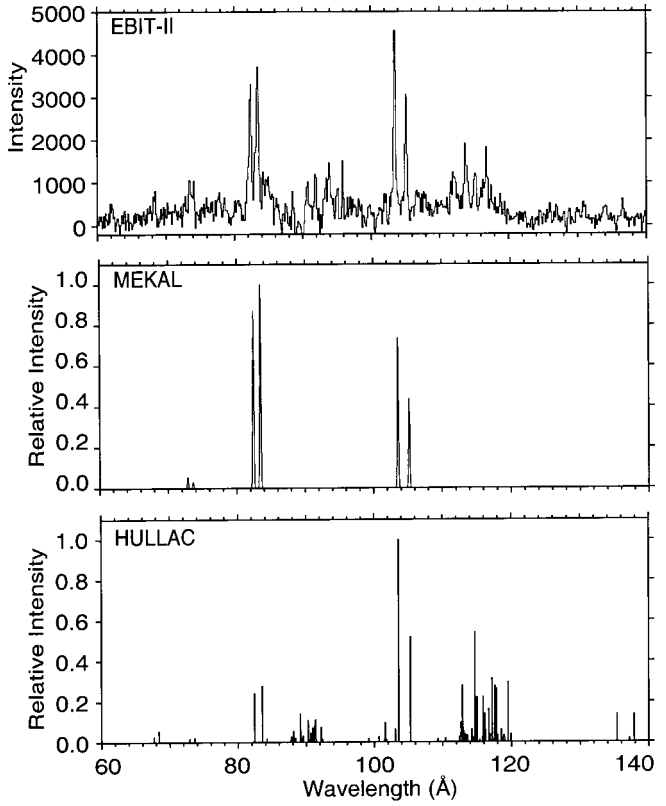

FIG. 6.—Spectrum of Fe IX from EBIT-II compared with synthetic spectra derived from MEKAL and HULLAC calculations.

errors introduced by the subtraction process. A summary of the results is given in Tables 1–4. Spectra from up to 41 runs were fitted to obtain the wavelengths of the lines from a given charge state. Errors in the wavelengths were computed as standard errors determined from line positions fitted in separate runs. This procedure yields a larger and, we believe, a more reliable estimate of error than that given by the counting statistics and the line width.

The measured line intensities given in Tables 1–4 were corrected for the response function of the spectrometer. Here we relied on a calibration of the spectrometer performed at Lawrence Berkeley National Laboratory's Advanced Light Source (Lepson et al. 2001).[2] Figure 8 shows the response function of the spectrometer, which peaks at 80 Å, and is dominated by the grating efficiency. The manipulations required to extract a "pure" charge state make those spectra statistically unsatisfactory, in part because of the increased noise, and in part because the subtractions can change the relative intensities and other details of the spectral emissivities. We therefore used the original spectra to determine line strengths of the lines that were identified with the use of the manipulated "pure" spectra. These line strengths were then corrected for the spectrometer response function and were given a relative strength of 1–20.

Where identification was possible, we have listed in Tables 1–4 the transition associated with a given feature.

[2] This report is available at http://www.llnl.gov/tid/Library.html.

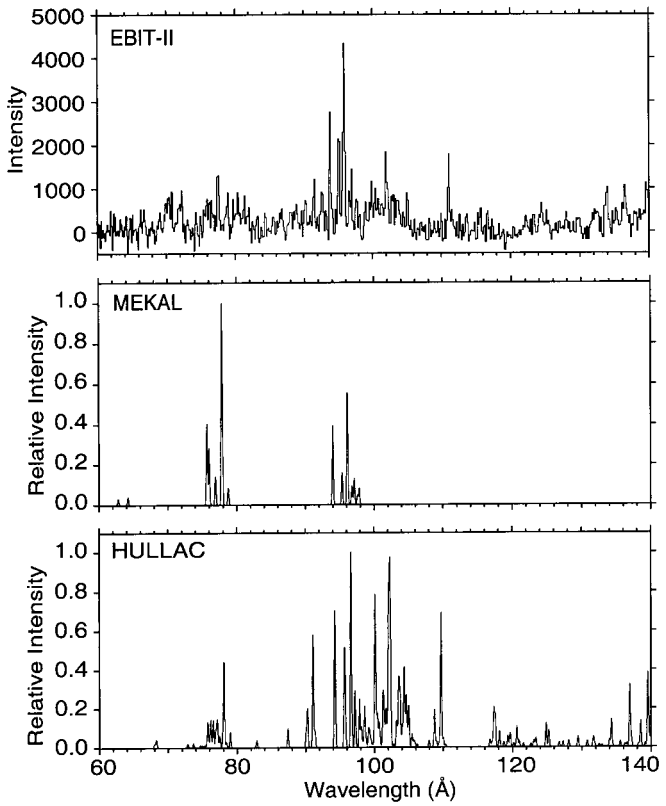

FIG. 7.—Spectrum of Fe X from EBIT-II compared with synthetic spectra derived from MEKAL and HULLAC calculations.

TABLE 1
SUMMARY OF Fe VII EMISSION DATA

Measured λ (Å)	Standard Error	Relative Intensity[a]	ID	Comment	Kelly λ[b] (Å)
100.70	0.064	1	...		...
101.76	0.055	1	...		...
102.64	0.024	3	...		...
103.62	0.014	3	...		...
105.12	0.031	5	...		...
106.44	0.015	4	$9f \rightarrow 3f$		...
107.01	0.027	1	...		...
108.55	0.017	3	$8f \rightarrow 3d$		⟨108.55⟩
110.67	0.023	3	...		...
111.73	0.012	8	$7f \rightarrow 3d$		111.74
117.01	0.020	10	$6f \rightarrow 3d$	Blend with VIII	⟨116.98⟩
117.22	0.010	10	$6f \rightarrow 3d$	Blend with VIII	⟨117.14⟩
119.69	0.034	4	$6f \rightarrow 3d$		119.69
120.68	0.027	2	$6f \rightarrow 3d$		120.64
121.55	0.025	1	...		121.55
124.38	0.015	2	...		⟨124.40⟩
124.93	0.015	2	...		⟨124.88⟩
125.44	0.052	2	...		⟨125.44⟩
126.57	0.020	2	...		⟨126.50⟩
127.22	0.012	20	$5f \rightarrow 3d$		127.26
127.59	0.023	16	$5f \rightarrow 3d$		⟨127.66⟩
128.83	0.028	9	$4s \rightarrow 3p$		...
129.64	0.024	9	$5f \rightarrow 3d$		⟨129.65⟩
130.04	0.004	6	$4s \rightarrow 3p$		130.05
130.27	0.017	20	$5f \rightarrow 3d$		⟨130.26⟩
132.48	0.055	5	$5f \rightarrow 3d$		132.41
133.86	0.048	5	$4s \rightarrow 3p$		⟨133.89⟩
139.27	0.043	9	$4s \rightarrow 3p$ (?)		...

NOTE.—Angle brackets denote a mean of several transitions.
[a] Scale 1–20.
[b] 1987.

Line identification was enabled in part by comparison with existing databases: MEKAL (Mewe-Kaastra-Liedahl; Kaastra & Mewe 1993; Mewe et al. 1995a) and Kelly (1987). The wavelengths from these databases are listed in Tables 1–4 for comparison. In addition, we made new calculations for Fe VIII–Fe X using the Hebrew University–Lawrence Livermore Atomic Code (HULLAC) (Bar-Shalom, Klapish, & Oreg 2001). The wavelengths from these calculations are also listed in Tables 2–4. Both the MEKAL database and the HULLAC calculations provide line intensity information and can thus be used to construct synthetic spectra for comparison with our measurements. These are shown for Fe VIII–Fe X in Figures 3, 6, and 7, respectively (MEKAL does not include Fe VII in the region we studied here, nor were any HULLAC calculations made for this charge state). MEKAL is based roughly on an astrophysically relevant temperature of 10^6 K and density of 10^{10} cm^{-3}, while HULLAC is based on a density of 10^{11} cm^{-3}. While Kelly (1987) also includes line intensity information, his values were obtained from laboratory samples with much higher densities than found in either EBIT-II or relevant astrophysical sources. Consequently, they often vary dramatically from intensities observed in the EBIT-II experiments, as well as astrophysical plasmas, and in most cases are not applicable. For this reason we do not include synthetic spectra derived from the Kelly database.

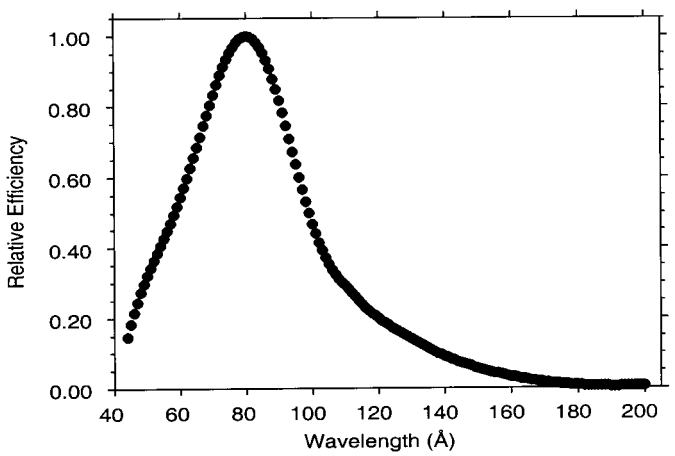

FIG. 8.—Response function, including both the grating and CCD, of the grazing-incidence flat-field spectrometer on EBIT-II, as derived from synchrotron measurements.

Unlike the entries in the tables, the spectra shown in Figures 1–7 have not been corrected for the response function because doing so greatly exaggerates unsightly noise at either end of the spectra, where the response function is weak. Instead, we used the response function of the detector to adjust the synthetic spectra derived from MEKAL and HULLAC so that the spectra are directly comparable with each other.

TABLE 2
SUMMARY OF Fe VIII EMISSION DATA

Measured λ (Å)	Standard Error	Relative Intensity[a]	ID	Comment	Kelly λ[b] (Å)	MEKAL λ[c] (Å)	HULLAC λ[d] (Å)	HULLAC Intensity[a]
82.95	0.010	1	...		...	...	...	...
83.51	0.011	1	...		...	...	...	...
86.37	0.027	1	$11f \rightarrow 3d$		...	...	...	...
87.33	0.018	1	$10f \rightarrow 3d$		...	...	...	...
88.64	0.014	1	$9f \rightarrow 3d$		...	...	...	...
89.47	0.041	1	$4d \rightarrow 3p$		...	...	89.14	<1
89.99	0.030	1	...		...	...	...	...
90.55	0.014	1	$8f \rightarrow 3d$		...	...	...	...
91.92	0.014	1	...		...	...	...	...
92.18	0.013	1	...		...	...	...	...
92.66	0.042	1	...		...	...	...	...
93.53	0.016	1	$7f \rightarrow 3d$		93.47	93.47	...	...
93.66	0.028	1	$7f \rightarrow 3d$		93.62	93.62	...	...
98.46	0.017	1	$6f \rightarrow 3d$		98.37	98.37	...	...
98.60	0.017	1	$6f \rightarrow 3d$		98.55	98.55	...	...
107.96	0.015	2	$5f \rightarrow 3d$		107.87	107.87	107.87	4
108.11	0.019	5	$5f \rightarrow 3d$		108.08	⟨108.08⟩	⟨108.08⟩	6
112.49	0.013	2	$4s \rightarrow 3p$		⟨112.48⟩	⟨112.48⟩	⟨112.48⟩	5
112.99	0.022	2	$4s \rightarrow 3p$		112.93	112.93	113.04	3
113.31	0.029	1	$4s \rightarrow 3p$		113.32	...	113.36	1
113.78	0.017	1	$4s \rightarrow 3p$		113.76	...	113.73	1
114.12	0.017	2	$4s \rightarrow 3p$		114.30	...	114.42	<1
116.25	0.016	2	$4s \rightarrow 3p$		116.20	...	116.63	2
117.04	0.022	2	$4s \rightarrow 3p$	Blend with VII	...	116.96	...	...
117.21	0.007	3	$4s \rightarrow 3p$	Blend with VII	117.20	117.2	117.69	3
118.97	0.007	1	$4s \rightarrow 3p$		118.91	118.91	118.99	1
119.57	0.031	2	$4s \rightarrow 3p$		119.38	119.38	119.45	2
	...	...	...		...	...	128.96	2
	...	...	...		...	...	130.54	1
130.99	0.020	4	$4f \rightarrow 3d$		130.94	130.94	130.94	13
131.25	0.009	20	$4f \rightarrow 3d$		⟨131.25⟩	⟨131.25⟩	⟨131.25⟩	20
133.28	0.035	3	$4f \rightarrow 3d$		...	...	...	...
	...	...	...		...	...	⟨134.40⟩	2
135.58	0.022	3	$4f \rightarrow 3d$		...	...	...	...
	...	...	...		...	...	136.84	<1

NOTE.—Angle brackets denote a mean of several transitions.
[a] Scale 1–20.
[b] 1987.
[c] Mewe, Kaastra, & Liedahl 1995a.
[d] Present calculations.

5. DISCUSSION

As shown in our earlier laboratory measurements (Beiersdorfer et al. 1999b; Lepson et al. 2000), commonly used spectral models are highly incomplete in the extreme-ultraviolet. This is in part because the wealth of possible transitions makes the calculations complex and time-consuming, and the lines are generally weak (especially when compared to the $n = 3$ to $n = 3$ lines near 170 Å); and in part because of the absence of laboratory observations of such low charge states. While in many cases this shortcoming was recognized, the locations, relative magnitudes, and collision strengths were not available, so models were unable to take these lines into account. The MEKAL database was found earlier to be more complete than other databases, such as the Arcetri Spectral Code (Landini & Monsignori Fossi 1990) and CHIANTI (Dere et al. 1997). Despite its higher level of completeness, the MEKAL synthetic spectra fail to fully reproduce the many emission lines seen with EBIT. Our HULLAC calculations show numerous lines not found in MEKAL, and they more closely reproduce the EBIT measurements. But these do not include lines originating from levels with high principal quantum number ($n > 6$), which may still be relevant since there are many lines with finite cross-sections that bunch up. Also, some of the predicted features differ significantly in strength from those found in EBIT. This may be in part due to uncertainties in the predicted line positions. Given the high density of lines, many features consist of more than one line. Calculations of the intensity of a given feature must, therefore, properly account for line blending. This is very difficult to accomplish, as the wavelength accuracy of the calculations is not sufficient in this regard. The calculations may, therefore, predict features with a different mix of lines than that observed.

For Fe VIII, MEKAL gives a decent representation of the Rydberg series up to the $7f \rightarrow 3d$ transitions but misses lines closer to the series limit. Overall, the MEKAL database is fairly good, and misses only flux in the lines from $n > 8$ and lines in the 110–140 Å region. Because the $n > 8$

TABLE 3
SUMMARY OF Fe IX EMISSION DATA

Measured λ (Å)	Standard Error	Relative Intensity[a]	ID	Comment	Kelly λ[b] (Å)	MEKAL λ[c] (Å)	HULLAC λ[d] (Å)	HULLAC Intensity[a]
59.88	0.026	1	...		...	...	...	...
60.86	0.137	1	...		...	...	...	...
62.13	0.131	2	$6d \rightarrow 3p$		...	...	...	...
68.36	0.099	2	$5d \rightarrow 3p$		...	...	68.32	1
72.85	0.042	1	$5s \rightarrow 3p$		⟨72.87⟩	72.85	72.85	<1
73.58	0.010	2	$5s \rightarrow 3p$		73.62	73.62	73.62	<1
77.88	0.021	3	...		...	...	...	...
78.62	0.023	2	...		...	...	...	...
79.13	0.099	2	...		...	...	...	...
80.80	0.081	2	...		...	...	...	...
82.41	0.023	7	$4d \rightarrow 3p$		82.43	82.43	82.43	5
83.46	0.008	7	$4d \rightarrow 3p$		83.46	83.46	83.45	5
84.41	0.022	2	...		...	...	...	...
84.73	0.023	3	...		...	...	...	...
85.11	0.020	2	...		...	...	...	...
85.68	0.018	2	...		...	...	...	...
	...	...	...		...	...	88.08	1
	...	...	...		...	...	89.15	3
	...	...	...		...	...	90.20	1
90.58	0.013	5	$5f \rightarrow 3d$		...	...	90.65	1
	...	...	...		...	...	90.89	1
	...	...	...		...	...	91.19	2
	...	...	...		...	...	91.36	2
91.98	0.027	5	$5f \rightarrow 3d$		...	...	92.13	1
93.59	0.013	5	$5f \rightarrow 3d$		...	...	...	...
94.07	0.023	6	$5f \rightarrow 3d$		...	...	...	...
102.23	0.027	7	$5f \rightarrow 3d$		...	...	101.55	1
103.55	0.007	20	$4s \rightarrow 3p$		103.57	103.57	103.57	20
105.20	0.007	15	$4s \rightarrow 3p$		105.21	105.20	105.21	10
106.80	0.101	6	...		...	...	...	...
107.10	0.021	5	...		...	...	...	...
110.30	0.071	3	...		...	...	...	...
111.75	0.010	6	$4f \rightarrow 3d$	Blend with VII	⟨111.75⟩	...	...	...
112.13	0.008	7	$4f \rightarrow 3d$		⟨112.06⟩	...	112.90	5
113.88	0.010	18	$4f \rightarrow 3d$		⟨113.98⟩	...	114.14	1
115.22	0.033	10	$4f \rightarrow 3d$		115.35	...	⟨114.80⟩	18
116.28	0.016	10	$4f \rightarrow 3d$		116.41	...	⟨115.95⟩	7
116.94	0.026	8	$4f \rightarrow 3d$		116.80	...	116.70	3
	...	...	...		...	...	⟨117.20⟩	6
117.51	0.046	6	$4f \rightarrow 3d$		...	...	117.60	6
	...	...	...		...	...	117.74	5
	...	...	...		...	...	118.52	1
118.96	0.009	6	$4f \rightarrow 3d$		...	...	119.53	6
134.08	0.025	13	$4f \rightarrow 3d$		...	...	135.32	3
136.70	0.027	9	$4f \rightarrow 3d$		...	...	137.86	3
	...	...	...		...	...	...	...
171.06	0.003	377	$3d \rightarrow 3p$		171.08	171.08	171.07	315

NOTES.—Angle brackets denote a mean of several transitions. Intensity exceeds 20 in the case of the strong 171 Å line, given for comparison.
[a] Scale 1–20.
[b] 1987.
[c] Mewe et al. 1995a.
[d] Present calculations.

lines fall into a narrow wavelength band near the series limit, their combined flux may become important, especially when applying global fitting procedures. This has been seen experimentally in iron L-shell X-ray spectra (Brown et al. 1998) and found to be of great importance in fitting the X-ray emission of Capella observed by *ASCA* (Brickhouse et al. 2000). HULLAC includes more of the weak lines seen with EBIT-II, but the calculations include lines only up to the $5f \rightarrow 3d$ transitions.

For Fe IX, MEKAL essentially includes only the strongest $4d \rightarrow 3p$ and $4s \rightarrow 3p$ transition lines. Although it does have the relatively weak $5s \rightarrow 3p$ lines, it has no listings of the many $4f \rightarrow 3d$ and $5f \rightarrow 3d$ transition lines clustered around 115 and 90 Å, respectively. Consequently, 79% of the flux observed for Fe IX on EBIT-II between 60 and 140 Å is absent from the MEKAL database, which lacks transitions from high principal quantum numbers. We have identified the locations of some of these transitions in our

TABLE 4
SUMMARY OF Fe X EMISSION DATA

Measured λ (Å)	Standard Error	Relative Intensity[a]	ID	Kelly λ[b] (Å)	MEKAL λ[c] (Å)	HULLAC λ[d] (Å)	HULLAC Intensity[a]
62.52	0.037	2	...	...	...	...	...
63.04	0.052	2	$5s \rightarrow 3p$	62.80	62.80	...	...
64.09	0.013	1	...	...	64.22	...	...
65.78	0.024	2	...	...	...	...	...
66.33	0.014	3	...	...	...	...	...
66.97	0.034	2	...	...	...	...	...
68.27	0.016	2	$4p \rightarrow 3s$	...	...	⟨68.28⟩	1
69.93	0.020	3	...	...	64.22	...	...
70.98	0.012	5	...	...	64.22	...	...
73.52	0.017	3	$4d \rightarrow 3p$	...	...	73.66	<1
75.84	0.042	2	$4d \rightarrow 3p$	75.68	75.68	75.74	2
76.11	0.037	2	$4d \rightarrow 3p$	76.01	76.01	76.18	3
	...	...	$4d \rightarrow 3p$	76.53	...	⟨76.52⟩	3
76.86	0.010	4	$4d \rightarrow 3p$	⟨76.87⟩	76.92	76.89	1
77.76	0.010	7	$4d \rightarrow 3p$	⟨77.84⟩	⟨77.84⟩	⟨78.06⟩	8
78.93	0.042	3	$4d \rightarrow 3p$	78.77	78.77	...	...
80.58	0.010	5	...	...	...	...	...
82.10	0.031	7	...	...	...	...	...
88.18	0.023	2	...	...	...	...	...
91.79	0.011	5	$4s \rightarrow 3p$	...	...	92.01	12
92.83	0.016	6	...	...	...	...	...
94.00	0.007	16	$4s \rightarrow 3p$	94.01	94.01	94.01	14
95.31	0.009	13	$4s \rightarrow 3p$	⟨95.36⟩	⟨95.36⟩	⟨95.36⟩	12
96.05	0.008	20	$4s \rightarrow 3p$	96.12	96.12	96.12	20
96.76	0.013	4	$4s \rightarrow 3p$	96.79	96.79	96.78	6
97.08	0.014	5	$4f \rightarrow 3d$	97.12	97.12	97.14	1
97.81	0.032	7	$4s \rightarrow 3p, 4f \rightarrow 3d$	⟨97.82⟩	⟨97.72⟩	⟨97.80⟩	22
99.99	0.009	9	$4f \rightarrow 3d$	...	...	⟨99.85⟩	35
100.57	0.017	4	...	...	...	...	...
102.18	0.010	10	$4f \rightarrow 3d$	102.19	...	⟨101.9⟩	7
111.23	0.010	8	$4p \rightarrow 3s$	...	...	111.11	14
124.50	0.031	6	...	...	...	...	...
134.09	0.022	10	$4p \rightarrow 3d$	...	...	⟨134.2⟩	3
136.69	0.015	5	$4p \rightarrow 3d$	...	...	136.33	4
139.30	0.030	10	$4p \rightarrow 3d$	...	...	138.95	2
139.81	0.042	11	$4p \rightarrow 3d$	...	...	⟨139.75⟩	4
	...	...	...	...	...	...	...
174.51	0.009	390	$3d \rightarrow 3p$	174.53	174.53	174.53	335

NOTES.—Angle brackets denote a mean of several transitions. Intensity exceeds 20 for the strong 174.5 Å line, given for comparison, and for some blended HULLAC lines, in which the intensities of several lines are added together.

[a] Scale 1–20.

[b] 1987.

[c] Mewe et al. 1995a.

[d] Present calculations.

spectra, based on extrapolations from the known transitions. New calculations were carried out with HULLAC that reproduce the large cluster of lines around 115 Å. These lines are ascribed to $4f \rightarrow 3d$ transitions. Similarly, by including the $n = 5$ complex in the calculations, HULLAC reproduces the cluster of lines at 90 Å, which we ascribe to $5f \rightarrow 3d$ transitions. As the intensity values in Table 3 illustrate, HULLAC underestimates line intensities for the $4d \rightarrow 3p$ lines and overestimates some of the $4f \rightarrow 3d$ lines. However, such discrepancies are minor compared to omitting the lines altogether from emission codes.

For Fe x, MEKAL includes the $4s \rightarrow 3p$, $5s \rightarrow 3p$, and $4d \rightarrow 3p$ lines. It does not include the many strong $4f \rightarrow 3d$ transition lines above 100 Å and the many weaker lines at 80–90 Å and below 75 Å from $n > 5$ levels. While many of the missing lines are relatively weak, their large number accounts for 81% of the flux observed between 60 and 140 Å. HULLAC provides a more accurate rendition of the Fe x emission. The HULLAC calculations have many more lines than MEKAL and include the many $4f \rightarrow 3d$ transitions in the 90–110 Å region. On closer inspection, however, it becomes difficult to completely correlate HULLAC's predicted transitions with the observed features. In many cases the predicted intensities differ dramatically from those observed, and wavelengths differ as well—by over 0.3 Å in several cases.

Differences in intensities between EBIT-II and HULLAC may be due to different blends and inaccurate wavelengths. In addition, without higher n transitions, the radiative cascade contributions are also lacking, as are some other excitation processes that can affect the flux. The calculation of relatively low charge states of iron is inherently difficult because of the many electron-electron interactions in the atomic structure and in the excitation that is very difficult to

account for. Moreover, HULLAC was not meant for such low charge states; even if all excitation processes had been included, the calculations would still be not as reliable as for higher charge states (Bar-Shalom et al. 2001).

It is interesting to make a quantitative estimate of the contribution of weak lines to the *EUVE* Procyon spectrum. The average photon flux over the range 80–140 Å attributed to continuum emission by Schrijver et al. (1995) is about 1.8×10^{-4} photon cm^{-2} s^{-1} Å^{-1} (see Fig. 1, Schmitt et al. 1996). Using the line fluxes of Fe IX λ171.06 and Fe X λ174.51 from Drake, Laming, & Widing (1995) to scale the measured line intensities, we estimate the weak-line flux, if attributed to continuum over the same spectral range, to be 5.1×10^{-5} photon cm^{-2} s^{-1} Å^{-1} for Fe IX and 3.86×10^{-5} photon cm^{-2} s^{-1} Å^{-1} for Fe X. From these two ions alone, the laboratory measurements account for 45% of the Schrijver et al. continuum. The theoretical values are similar, accounting for 39% of the flux. These results strongly support the analysis of Schmitt et al. (1996).

6. SUMMARY

In summary, as suggested by Jordan (1968, 1996), Schmitt et al. (1996), and Drake et al. (1997), and demonstrated by laboratory measurements by Beiersdorfer et al. (1999b), published spectral modeling codes do not adequately reproduce the wealth of Fe VII–Fe X lines in the extreme-ultraviolet needed for global fitting models. We have presented measured emission line spectra of the individual ions, along with new calculations that aid inline identifications. Wavelength and relative intensity comparisons between the measured and calculated spectra show relatively good qualitative agreement. We have estimated from laboratory measurements that weak lines from Fe IX and X alone account for nearly half of the *EUVE* Procyon spectral flux previously attributed to continuum emission; other M-shell ions are likely to contribute an additional significant fraction. Because of the high density of lines in this spectral band, it is at present nearly impossible to correlate all the calculated lines with those that we observed. But exact correlation and identification are not necessary, as most lines are weak and blended. Despite a somewhat higher resolving power than our present measurements, identifying these lines in *Chandra* spectra, for example, would be impractical, given the weakness of the lines and the limitations on observing time. On EBIT-II, we find that the strongest $n = 4 \rightarrow n = 3$ lines are about 15–20 times weaker than the $n = 3 \rightarrow n = 3$ lines at 171 Å and above. In a true Maxwellian plasma this difference will increase to a factor of 40 or 50. However, because they are numerous, their combined flux is considerable. The error made by including these lines in spectral models without proper identification is likely to be much less than omitting them altogether. If the strongest line of a given iron charge state is observed in a spectrum, then a representation of the many weaker lines must be included in the global fit as well, lest most of the flux be omitted. Moreover, the preponderance of weak lines is also relevant to single line based fittings, as one must take care to properly fit the pseudo-continuum or "pedestal" on which a given line sits.

Given that the databases for the higher charge states of iron (Fe XI–Fe XVI) are similarly devoid of the type of transitions that were found to be important for Fe VIII–Fe X, we can safely assume that measurements need to be performed to assess the missing flux and identify the relevant transitions. In fact, we illustrated this already for Fe XIII (Lepson et al. 2000). Measurements are in preparation to extend our laboratory studies to Fe XI–Fe XVI in order to generate the relevant line lists.

This work was supported by a Space Astrophysics Research and Analysis grant from NASA and was performed under the auspices of the Department of Energy by the University of California Lawrence Livermore National Laboratory under contract W-7405-ENG-48. Space Research Organization Netherlands is supported financially by NWO.

REFERENCES

Bar-Shalom, A., Klapisch, M., & Oreg, J. 2001, J. Quant. Spectrosc. Radiat. Transfer, 71, 169
Beiersdorfer, P., Crespo López-Urrutia, J. R., Springer, P., Utter, S. B., & Wong, K. L. 1999a, Rev. Sci. Instrum., 70, 276
Beiersdorfer, P., Lepson, J. K., Brown, G. V., Utter, S. B., Kahn, S. M., Liedahl, D. A., & Mauche, C. W. 1999b, ApJ, 519, L185
Beiersdorfer, P., et al. 2000, Rev. Mexicana Astron. Astrofis., 9, 123
Brickhouse, N. S., Dupree, A. K., Edgar, R. J., Liedahl, D. A., Drake, S. A., White, N. E., & Singh, K. P. 2000, ApJ, 530, 387
Brown, G. V., Beiersdorfer, P., Liedahl, D. A., Kahn, S. M., & Widmann, K. 1998, ApJ, 502, 1015
Dere, K. P., Landi, E., Mason, H. E., Monsignori Fossi, B., & Young, P. R. 1997, A&AS, 125, 149
Drake, J. J., Laming, J. M., & Widing, K. G. 1995, ApJ, 443, 393
———. 1997, ApJ, 478, 403
Harada, T., & Kita, T. 1980, Appl. Opt., 19, 3987
Jordan, C. 1968, J. Phys. B, 1, 1004
Jordan, C. 1996, in IAU Colloq. 152, Astrophysics in the Extreme Ultraviolet, ed. S. C. Bowyer & R. F. Malina (Boston: Kluwer), 81
Kaastra, J. S., & Mewe, R. 1993, Legacy, 3, 6
Kelly, R. L. 1987, J. Phys. Chem. Ref. Data, 16, S1
Landini, M., & Monsignori Fossi, B. C. 1990, A&AS, 82, 229
Lepson, J. K., Beiersdorfer, P., Brown, G. V., Chen, H., Gullikson, E. M., Schneider, M. B., Utter, S. B., & Wong, K. L.. 2001, Univ. California Lawrence Livermore Natl. Lab. Rep. UCRL-ID-142264
Lepson, J. K., Beiersdorfer, P., Brown, G. V., Kahn, S. M., Liedahl, D. A., Mauche, C. W., & Utter, S. B. 2000, Rev. Mexicana Astron. Astrofis., 9, 137
Mewe, R., Kaastra, J. S., & Liedahl, D. A. 1995a, Legacy, 6, 16
Mewe, R., Kaastra, J. S., Schrijver, C. J., van den Oord, G. H. J., & Alkemade, F. J. M. 1995b, A&A, 296, 477
Nakano, N., Kuroda, H., Kita, T., & Haroda, T. 1984, Appl. Opt., 23, 2386
Schmitt, J. H. M. M., Drake, J. J., & Stern, R. A. 1996, ApJ, 465, L51
Schrijver, C. J., Mewe, R., van den Oord, G. H. J., & Kaastra, J. S. 1995, A&A, 302, 438